Mixing of two co-directional Rayleigh surface waves in a nonlinear elastic material

Merlin B. Morlock, Jin-Yeon Kim, and Laurence J. Jacobs[a)]
School of Civil and Environmental Engineering, Georgia Institute of Technology, Atlanta, Georgia 30332-0355

Jianmin Qu
Department of Civil and Environmental Engineering, Northwestern University, Evanston, Illinois 60208-3109

(Received 27 June 2014; revised 28 October 2014; accepted 22 November 2014)

The mixing of two co-directional, initially monochromatic Rayleigh surface waves in an isotropic, homogeneous, and nonlinear elastic solid is investigated using analytical, finite element method, and experimental approaches. The analytical investigations show that while the horizontal velocity component can form a shock wave, the vertical velocity component can form a pulse independent of the specific ratios of the fundamental frequencies and amplitudes that are mixed. This analytical model is then used to simulate the development of the fundamentals, second harmonics, and the sum and difference frequency components over the propagation distance. The analytical model is further extended to include diffraction effects in the parabolic approximation. Finally, the frequency and amplitude ratios of the fundamentals are identified which provide maximum amplitudes of the second harmonics as well as of the sum and difference frequency components, to help guide effective material characterization; this approach should make it possible to measure the acoustic nonlinearity of a solid not only with the second harmonics, but also with the sum and difference frequency components. Results of the analytical investigations are then confirmed using the finite element method and the experimental feasibility of the proposed technique is validated for an aluminum specimen.
 [http://dx.doi.org/10.1121/1.4904535]

[ANN] Pages: 281–292

I. INTRODUCTION

Nonlinear acoustic techniques have proven to be very useful in detecting microstructural changes within a solid for which linear techniques are not sensitive enough.[1,2] These nonlinear techniques are often based on the measurement of a second harmonic contribution in order to determine the acoustic nonlinearity of a material—when an initially monochromatic sinusoidal wave propagates through a nonlinear solid, higher harmonic wave components are generated. As an alternative, recent experiments[3,4] successfully used wave mixing techniques for bulk waves to generate new waves according to the theory of Jones and Kobett from 1963.[5] As the use of Rayleigh waves has demonstrated several advantages in nonlinear ultrasonic experiments with a single fundamental wave,[6,7] the idea of the present paper is to mix two such waves. The current research considers the utility of wave mixing of two Rayleigh waves propagating in the same direction, denoted as co-directional. Here, one not only obtains higher harmonics of each fundamental wave, but also the sums and differences of all the harmonic frequencies (combination frequencies); these additional frequency components provide alternative ways to measure the acoustic nonlinearity of a material which can be beneficial. For example, with similar fundamental frequencies, a small difference frequency is obtained which is less attenuated than the corresponding second harmonics. Also, such wave mixing techniques are relatively immune to the instrumentation nonlinearity that can dominate second harmonic generation measurements which typically use a single, fundamental input frequency which corresponds to the center frequency of the exciting transducer.

In 1981 Kalyanasundaram published results[8] on the nonlinear theory of the mixing of two co-directional Rayleigh waves. The current research considers an analytical model similar to Kalyanasundaram by building on Jones and Kobett,[5] plus the nonlinear theory of a single fundamental Rayleigh wave provided by Zabolotskaya.[9,10] Zabolotskaya proposed a unique approach based on the Hamiltonian formalism to derive the differential equations for the amplitudes of the included frequency components. An advantage of this energy based approach is the use of a variable number of frequency components as opposed to the results of Kalyanasundaram[8] where only six frequency components are considered. This flexibility is crucial to easily incorporate a large number of frequency components, which enables the representation of highly nonlinear phenomena such as shock formations. In contrast to related literature,[8–11] the current research develops a model without the need for the slowly varying envelope approximation (SVEA), which results in more accurate calculations. Next, the inclusion of diffraction effects in the parabolic approximation gives an analytical model similar to that of Shull *et al.*[12] but for the case of two co-directional Rayleigh waves which has not been published yet in this form. In addition, the effects of

[a)]Author to whom correspondence should be addressed. Also at: G. W. Woodruff School of Mechanical Engineering, Georgia Institute of Technology, Atlanta, GA 30332-0360. Electronic mail: laurence.jacobs@coe.gatech.edu

different amplitudes and frequencies of the fundamental waves and of the corresponding ratios are discussed. Formulas are derived to calculate the acoustic nonlinearity of a material similar to the case of a single fundamental Rayleigh wave investigated by Herrmann *et al.*,[6] but not only based on the second harmonics but also on the sum and difference frequency components. Finally, results from the analytical model are compared to results from a finite element model for validation purposes.

The overall objective of this research is to provide models that support experiments and enable the interpretation of the measured data and the selection of the amplitudes and frequencies of the two fundamental waves, in order to maximize the amplitudes of the second harmonics, as well as those of the sum and difference frequency components. This can help to enhance measurements by providing an improved signal-to-noise ratio (SNR), which enables a more accurate determination of the acoustic nonlinearity of a material; this research demonstrates the feasibility and potential of co-directional Rayleigh wave mixing in order to experimentally quantify the acoustic nonlinearity of a solid, analogously to longitudinal waves, in multiple ways within a single measurement.

II. ANALYTICAL MODEL

A. Modeling

Consider an isotropic, homogeneous, elastic and weakly nonlinear material. In order to determine significant solutions to the nonlinear Rayleigh wave equation, it is a good approximation to only take frequency components into account for which resonance is fulfilled. It is assumed in the following that the resonance condition of Jones and Kobett[5] holds similarly for Rayleigh waves which can be written as

$$\frac{(\omega_a \pm \omega_b)\mathbf{p}}{c} = \mathbf{k}_a \pm \mathbf{k}_b \overset{|\mathbf{p}|=1}{\rightarrow} \frac{|\omega_a \pm \omega_b|}{c} = |\mathbf{k}_a \pm \mathbf{k}_b|. \tag{1}$$

Here, c is the wave speed, $\mathbf{p}$ the propagation direction, $|\omega_a \pm \omega_b|$ the angular frequency, and $|\mathbf{k}_a \pm \mathbf{k}_b|$ the wavenumber of the generated and significant wave. Moreover, $\mathbf{k}_a$ and $\mathbf{k}_b$ as well as ω_a and ω_b are the wave vectors and angular frequencies of the two fundamental waves that are mixed. The absolute values $|\mathbf{k}_a| = k_a$ and $|\mathbf{k}_b| = k_b$ are the corresponding wavenumbers. As we are interested in nonlinear ultrasonic measurements where fundamental Rayleigh waves are compared to nonlinearly generated Rayleigh waves, we want this generation to be directly out of the interaction of the fundamentals to obtain larger amplitudes and a better SNR. Consequently, the wave speed c of the generated wave within Eq. (1) is set to the Rayleigh wave speed c_r which results in

$$(\omega_a \pm \omega_b)^2 = \omega_a^2 + \omega_b^2 \pm 2\omega_a\omega_b \cos(\Theta), \tag{2}$$

where Θ is the angle between the fundamental wave vectors. This leads to $\cos(\Theta) = 1$ and confirms that the resonance condition is only fulfilled for co-directional mixing.

As the individual fundamentals also fulfill the resonance condition which leads to second harmonics, it can be concluded that both of the second harmonics as well as the sum and difference frequency components are directly generated from the fundamentals, and are therefore of critical interest for experiments. By generalizing the co-directional mixing of the two fundamentals, it follows that the generated waves interact again with all other waves leading to the formation of all kinds of higher harmonics and combination frequencies. They can be written as $n\omega_a$, $m\omega_b$, and $|n\omega_a \pm m\omega_b|$ for $n = 1, 2, 3$, and $m = 1, 2, 3$. Moreover, it is assumed that the solution of the nonlinear problem is close to the solution of the corresponding linear problem.[9] Consequently, the solution form for the displacements in the x- and z-directions for co-directional Rayleigh wave mixing in a semi-infinite solid in the $z < 0$ half-space with the surface at $z = 0$ can be written as

$$u_x = \sum_n \underbrace{b_n e^{-in\omega_a t}}_{a_n} \underbrace{i\frac{n}{|n|}\left(\xi_1 e^{|n|k_a\xi_1 z} + \eta e^{|n|k_a\xi_2 z}\right) e^{ink_a x}}_{u_{xn}}, \tag{3a}$$

$$u_z = \sum_n \underbrace{b_n e^{-in\omega_a t}}_{a_n} \underbrace{\left(e^{|n|k_a\xi_1 z} + \eta\xi_2 e^{|n|k_a\xi_2 z}\right) e^{ink_a x}}_{u_{zn}}. \tag{3b}$$

The material dependent constants η, ξ_1, and ξ_2 are defined elsewhere.[9] The imaginary unit is denoted by i and all waves propagate in the positive x-direction. The variable b_n represents the displacement amplitudes of the different frequency components that are in demand. Moreover, each n describes a distinct frequency component, and negative n are the corresponding complex conjugates resulting in $a_n^* = a_{-n}$ and $b_n^* = b_{-n}$.

One thing that distinguishes Eqs. (3a) and (3b) from the work of Kalyanasundaram[8] is that all frequency components are pulled into only one summation for each displacement direction. This leads to a special definition of the control variable n. With the frequency mixing ratio (FMR) $\phi = \omega_b/\omega_a$ and $0 < \phi < 1$ without loss of generality, n takes the values

$$\begin{aligned}&\pm 1, \pm 2, \ldots, \pm\phi, \pm 2\phi, \ldots, \pm 1 \pm \phi, \pm 2 \pm \phi, \pm 1 \pm 2\phi,\\ &\pm 2 \pm 2\phi, \ldots, \pm 1 \mp \phi, \pm 2 \mp \phi, \pm 1 \mp 2\phi, \pm 2 \mp 2\phi, \ldots .\end{aligned} \tag{4}$$

Integers and multiples of ϕ represent harmonics, whereas the other terms denote combination frequency components. The zero frequency is not considered.

As Eqs. (3a) and (3b) are analogous to the solution form Zabolotskaya postulated,[9] we can take advantage of the corresponding derivation to solve for the unknown and varying b_n. To follow the approach of Zabolotskaya in obtaining the kinetic and elastic energy, one needs to integrate over a distance in the x-direction that contains full periods of all frequencies involved. If ω_a and ω_b are decimals with a finite number of decimal places, fractions of such decimals or if numbers with infinite decimal places cancel out in the FMR,

then one can always find such a distance. When such a general case is considered, the kinetic energy $\mathcal{T}$ as well as the elastic energies $\mathcal{V}$ and $\mathcal{W}$ can be written analogously to Zabolotskaya[9] but with n given in Eq. (4). The energies are then used for the Lagrange equations of the second kind for the so far conservative system. The Lagrangian follows as $\mathcal{L}=\mathcal{T}-\mathcal{V}-\mathcal{W}$ and the different a_{-n} are chosen as generalized coordinates. Based on the expressions used by Zabolotskaya,[9] the generalized momenta $\partial\mathcal{L}/\partial\dot{a}_{-n}$ are equal to $\partial\mathcal{T}/\partial\dot{a}_{-n}=M\dot{a}_n/(2|n|)$. The other necessary term for the equations of motion is given by $\partial\mathcal{L}/\partial a_{-n}=-\partial\mathcal{V}/\partial a_{-n}-\partial\mathcal{W}/\partial a_{-n}$. Here, $\partial\mathcal{V}/\partial a_{-n}=M\omega_a^2|n|a_n/2$ holds, where M depends on material properties and contains the wavenumber k_{a}. In order to calculate the partial derivative of $\mathcal{W}$ with respect to a_{-n},

$$\mathcal{W}=\mu k_a^2\sum_{n=m+l}w_{nlm}a_{-n}a_m a_l \tag{5}$$

is utilized, where n has been replaced by $-n$ within the summation when compared to Zabolotskaya.[9] Note that w_{nlm} stays unchanged as it only contains absolute values of n and the condition $n=m+l$ needs to be fulfilled. This yields

$$\frac{\partial\mathcal{W}}{\partial a_{-n}}=-|n|\mu k_a^2\sum_{n=m+l}mlS_{ml}b_m b_l e^{-i(m+l)\omega_a t}. \tag{6}$$

The variables w_{nlm} as well as S_{ml}, given by Zabolotskaya,[9] solely depend on material properties and μ denotes the shear modulus of the solid. Also, m and l are control variables like n. This leads to the Lagrange equations of the second kind of

$$\begin{aligned}\frac{M}{2|n|}\left(\ddot{b}_n-2in\omega_a\dot{b}_n-n^2\omega_a^2 b_n\right)e^{-in\omega_a t}&=-\frac{M\omega_a^2}{2}|n|b_n e^{-in\omega_a t}+|n|\mu k_a^2\\&\quad\times\sum_{n=m+l}mlS_{ml}b_m b_l e^{-i(m+l)\omega_a t}.\end{aligned} \tag{7}$$

Making the assumption of periodic steady-state waves,[9] i.e., $\partial b_n/\partial t=\partial^2 b_n/\partial t^2=0$, one can evaluate the total derivative $\dot{b}_n=\partial b_n/\partial t+c_{\mathrm{r}}\partial b_n/\partial x=c_{\mathrm{r}}\partial b_n/\partial x$. Similarly, $\ddot{b}_n=c_r^2\partial^2 b_n/\partial x^2$. Based on these expressions, a multiplication of Eq. (7) with $e^{in\omega_a t}$ gives

$$-\frac{1}{2ink_a}\frac{\partial^2 b_n}{\partial x^2}+\frac{\partial b_n}{\partial x}=\frac{in\mu\omega_a}{Mc_r^3}\sum_{n=m+l}mlS_{ml}b_m b_l-\alpha n^2 b_n. \tag{8}$$

Here, an attenuation term has been implemented analogously to the literature[9,13] with the attenuation coefficient α. The first term on the right-hand side describes wave interactions caused by both geometric and material nonlinearities that lead to the generation of higher harmonics and combination frequency components. Equation (8) represents a system of coupled second order ordinary differential equations with quadratic terms, since the incorporated elastic energy is of cubic order.

As a next step, the time derivatives of the displacements need to be established to investigate particle velocities later on. They are similar to Zabolotskaya[9] given by

$$\dot{u}_x=v_x=\sum_n v_n e^{-in\omega_a t}u_{xn}e^{ink_a x}, \tag{9a}$$

$$\dot{u}_z=v_z=\sum_n v_n e^{-in\omega_a t}u_{zn}e^{ink_a x}, \tag{9b}$$

with the particle velocity amplitude of the different frequency components $v_n=c_r\partial b_n/\partial x-in\omega_a b_n$.

In a case where the amplitudes of the frequency components under consideration change slowly, it is common to use the SVEA.[8–11] This means that if $|\partial^2 b_n/\partial x^2|\ll|2nk_a\partial b_n/\partial x|$ holds the highest order derivative $\partial^2 b_n/\partial x^2$ can be neglected[14] within Eq. (8). The result is equivalent to Zabolotskaya's formula for a single fundamental wave,[9] but with a different definition of n and the equation is formulated with b_n instead of v_n. With the SVEA these amplitudes are related by[9]

$$v_n=-in\omega_a b_n. \tag{10}$$

B. Simulation

A characteristic quantity in wave propagation is the discontinuity distance which will be used for numerical analyses. At this distance, the slope of the waveform of the particle velocity becomes infinitely large for a hypothetical lossless nonlinear material.[15] Based on the discontinuity distances for a single fundamental bulk wave[13] and a single fundamental Rayleigh wave,[16] the empirical formula for the discontinuity distance of two co-directionally mixed Rayleigh waves can be written as

$$x_d=\frac{Mc_r^3}{8\mu|S_{11}|\omega_a(|b_{\mathrm{IC}a}|+\phi|b_{\mathrm{IC}b}|)}, \tag{11}$$

where S_{11} denotes S_{ml} for $m=l=1$. This equation is related to the expression for a single fundamental bulk wave by Eq. (21) and to the expression for a single fundamental Rayleigh wave by Eq. (10). The quantities $b_{\mathrm{IC}a}$ and $b_{\mathrm{IC}b}$ denote the initial values of b_1 and b_ϕ and the ratio $b_{\mathrm{IC}b}/b_{\mathrm{IC}a}$ is called the amplitude mixing ratio (AMR).

To reduce the computational complexity at highly nonlinear effects such as shocks, the SVEA will be utilized for the simulation of Eq. (8) in the following. Here, the behavior of the waveforms and the development of the displacement amplitudes in the case of low attenuation will be simulated numerically with MATHEMATICA 9.0.

1. Waveforms

For an easier comparison to the behavior of a single fundamental Rayleigh wave, assume the same steel material properties as in the literature[9] which are given in Table I. The amplitudes $b_{\mathrm{IC}a}$ and $b_{\mathrm{IC}b}$ are chosen of the same dimension as the fundamentals of longitudinal waves.[17] The initial amplitudes of all other frequency components are set to zero. Moreover, it is crucial to select low values for the attenuation

TABLE I. Material properties.

Material	Young's modulus E	Poisson's ratio σ	Mass density ρ	Third order elastic constants A, B, C		
Steel	$2 \times 10^{11}\,\mathrm{N/m^2}$	0.27	$7850\,\mathrm{kg/m^3}$	$-7.6 \times 10^{11}\,\mathrm{N/m^2}$	$-2.5 \times 10^{11}\,\mathrm{N/m^2}$	$-9 \times 10^{10}\,\mathrm{N/m^2}$
Fused quartz	$7.17 \times 10^{10}\,\mathrm{N/m^2}$	0.17	$2203\,\mathrm{kg/m^3}$	$-5.28 \times 10^{10}\,\mathrm{N/m^2}$	$5.4 \times 10^{10}\,\mathrm{N/m^2}$	$2.15 \times 10^{11}\,\mathrm{N/m^2}$
Aluminum	$7.09 \times 10^{10}\,\mathrm{N/m^2}$	0.34	$2700\,\mathrm{kg/m^3}$	$-3.5 \times 10^{11}\,\mathrm{N/m^2}$	$-1.5 \times 10^{11}\,\mathrm{N/m^2}$	$-1.03 \times 10^{11}\,\mathrm{N/m^2}$

coefficient to be able to observe effects such as shock formations before the waves decay. However, a simulation with a very small attenuation coefficient can be numerically difficult to handle and consequently a balance should be found.

The waveforms of the particle velocities are illustrated in Fig. 1 for two different FMRs. Here, all plots are normalized to v_{x0} which denotes the initial amplitude of v_x. The horizontal axis represents the dimensionless variable $\tau = \omega_a(t - x/c_r)/2\pi$. In plots (a1) and (b1) the horizontal velocity component forms a shock while in plots (a2) and (b2) a pulse arises in the vertical velocity component with an increasing propagation distance x. This behavior has been similarly shown by Zabolotskaya[9] but not for the case of co-directional Rayleigh wave mixing as presented here. Moreover, these effects occur independently of the FMR. The increased peaks indicate that the energy is shifted to the surface when higher frequencies are generated since they have lower penetration depths.[9,10] Additionally, the largest peaks get larger for a higher FMR. In contrast, very different fundamental frequencies lead to less sharp peaks as they have different energy transfer characteristics and do not form a shock and pulse at similar propagation distances in the case of comparable initial fundamental displacement amplitudes. Therefore, the amplitudes in plots (b1) and (b2) will decline until the smaller fundamental frequency generates a second shock and pulse, at propagation distances that are larger than the illustrated ones.

In addition, a shock and pulse can be formed independently of the AMR and for large FMRs as in (a1) and (a2) a beat can occur.

2. Displacement amplitudes

In the following, the development over the propagation distance of the displacement amplitudes b_n of the fundamentals, second harmonics as well as of the sum and difference frequency components is discussed. They are typically the largest, and therefore the most attractive components in

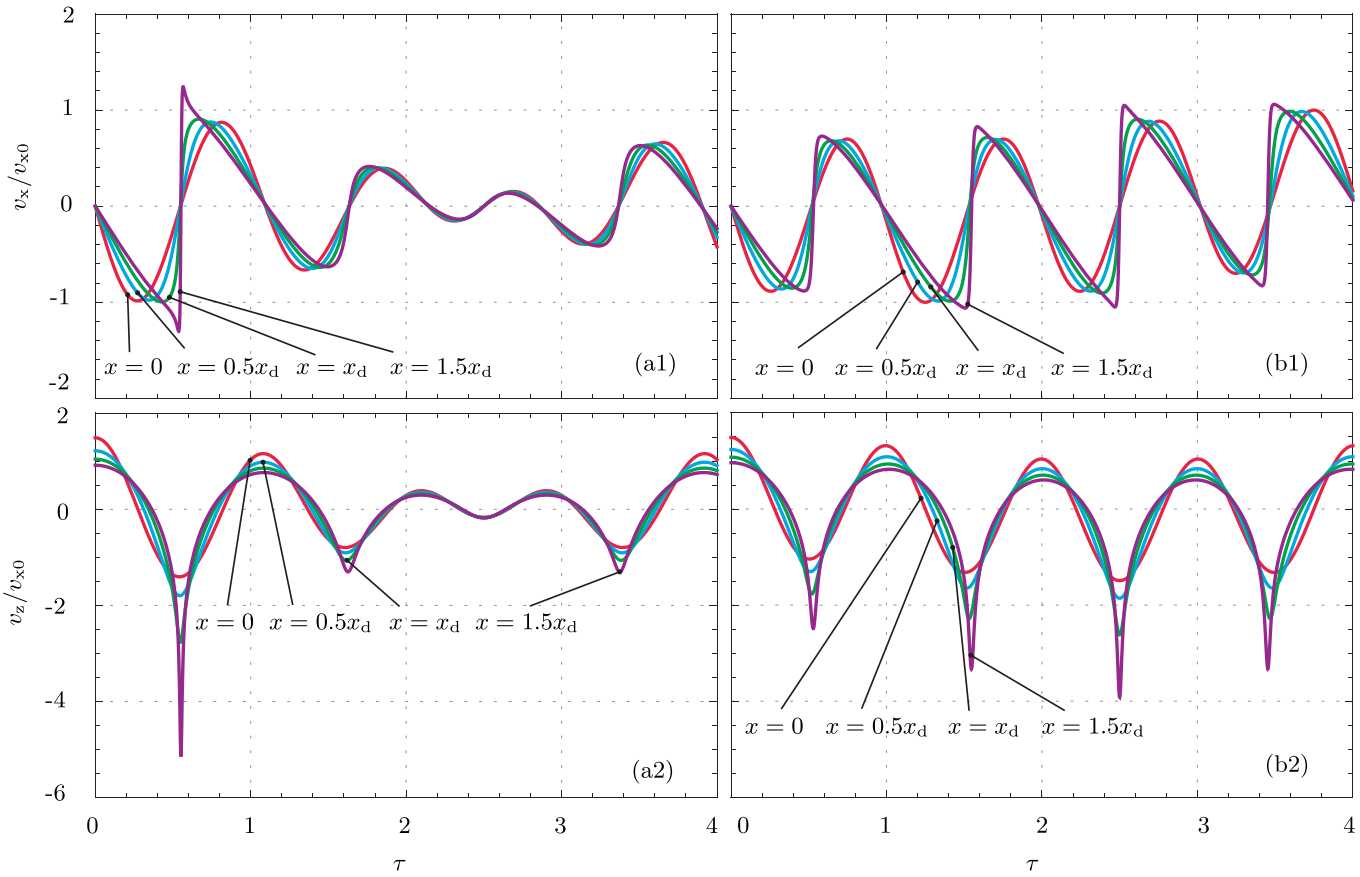

FIG. 1. (Color online) Normalized waveforms of the horizontal (a1), (b1) and the vertical (a2), (b2) particle velocity component at $z = 0$. The attenuation coefficient is set to $\alpha = 6 \times 10^{-4}\,\mathrm{Np/m}$ and the fundamental frequency $\omega_a = 5\pi \times 10^6\,\mathrm{rad/s}$ is fixed while $\omega_b = 4\pi \times 10^6\,\mathrm{rad/s}$ (a1), (a2) as well as $\omega_b = \pi \times 10^6\,\mathrm{rad/s}$ (b1), (b2). The initial conditions are chosen as $b_{\mathrm{IC}a} = b_{\mathrm{IC}b} = i7.5 \times 10^{-10}$ m. All frequencies up to the 120th harmonic of each fundamental wave and all combination frequencies up to $60\omega_a \pm 60\omega_b$ are included.

nonlinear ultrasonic measurements. Simulations are performed for fused quartz given in Table I to facilitate comparisons to Kalyanasundaram.[8] The results for two different FMRs are illustrated in Fig. 2. As purely imaginary values for b_{ICa} and b_{ICb} are utilized, the different b_n also remain as imaginary—this is analogous to the findings of Kalyanasundaram.[8] The reason for this behavior is that the change of the displacement amplitudes $\partial b_n/\partial x$ within the simulated equations equals an imaginary quantity.

The plots show that the energy transfer is larger for higher frequencies. On the one hand this means that the attenuation is obviously larger for higher frequencies, which can be observed, among others, for the difference frequency component at large propagation distances. On the other hand, the absolute value of the slope for small propagation distances tends to be larger if the frequency under consideration is higher (and the corresponding fundamental frequencies in the case that a non-fundamental component is investigated). Thus, the initial slopes of the $2\omega_b$ and the sum frequency components are larger in plot (a), since these and the corresponding fundamental ω_b component have higher frequencies.

A more complicated behavior is present within the initial development of the difference frequency component—as a high FMR results in a small difference frequency, and vice versa, the development of the difference frequency component depends on a balance of its own frequency and the fundamental frequencies. Therefore, the negative rise within plots (a) and (b) appears to be pretty much the same for small propagation distances.

These results are partially in line with the work of Kalyanasundaram.[8] The ω_b component changes more slowly for small FMRs in both models. For the sum and difference frequency components, the signs and the dependence of the initial slope on the FMR match relatively well. However, Kalyanasundaram states that for larger FMRs, the fundamentals as well as the sum and difference frequency components reach their first minima or maxima faster. This is not the case for the ω_a and the difference frequency components in the plots presented here. Also note that the overall behavior of the ω_a component is quite different. These discrepancies could be due to differing simulation parameters and modeling approaches. Especially, the number of included frequency components can be important if the propagation distances are large enough. Investigations have shown that for the utilized setups and considered propagation distance, more frequency components than only the fundamentals, second harmonics as well as the sum and difference frequencies as included by Kalyanasundaram are necessary to obtain an accurate development of these six components.

C. Implementation of diffraction effects

In addition to the nonlinear interaction and attenuation, diffraction effects can also be important to account for in nonlinear Rayleigh wave experiments, since they are often conducted in the far field where these effects might have a significant influence. Consequently, the model derived is extended to include these diffraction effects. Additionally, the SVEA is applied again to simplify the modeling and the computations as a system of coupled partial differential equations will be obtained and numerically solved.

The starting point of the derivation is the assumption of narrow angle diffraction which can be described using a parabolic approximation.[12,18] Suppose that the wave vector of diffracted Rayleigh waves can be written as $n\mathbf{k}_a = n(k_x, k_y, 0)^T$. Then the introduction of the small angle δ between the wave propagation direction and the x axis yields $nk_x = nk_a\cos(\delta)$ and $nk_y = nk_a\sin(\delta)$. These wavenumbers can be approximated with a Taylor series around $\delta = 0$ as $nk_x \approx nk_a(1 - \delta^2/2)$ and $nk_y \approx nk_a\delta$. The solution form of Eqs. (3a) and (3b) follows now as

$$u_x = \sum_n \underbrace{b_n e^{ink_a(-\delta^2 x/2+\delta y)}}_{b_{dn}} u_{xn} e^{in(k_a x-\omega_a t)}, \tag{12a}$$

$$u_z = \sum_n \underbrace{b_n e^{ink_a(-\delta^2 x/2+\delta y)}}_{b_{dn}} u_{zn} e^{in(k_a x-\omega_a t)}, \tag{12b}$$

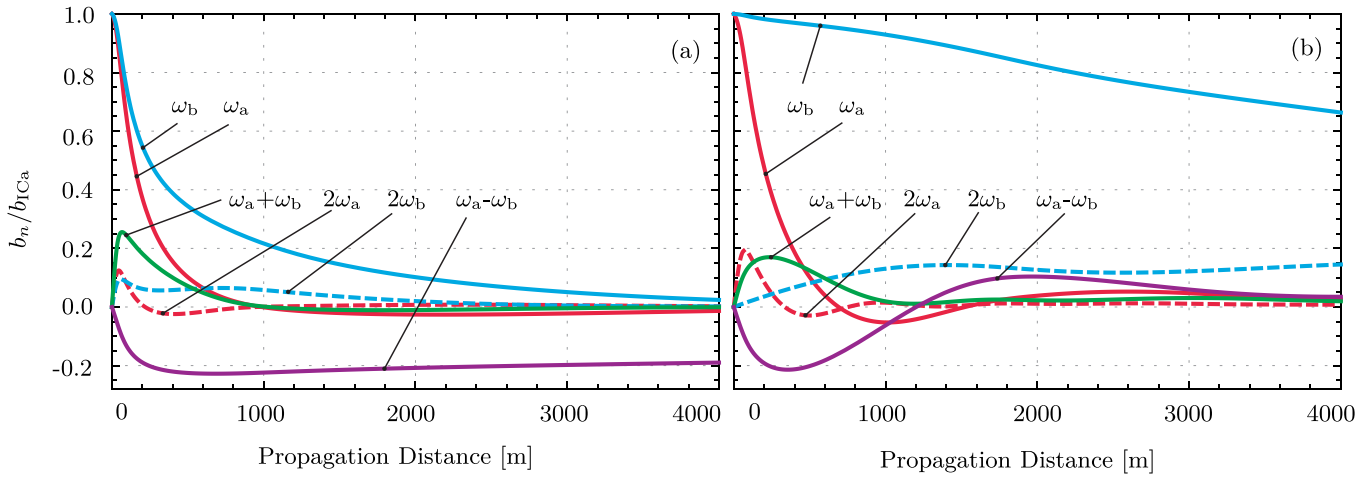

FIG. 2. (Color online) Normalized displacement amplitudes of selected frequency components over the propagation distance. The attenuation coefficient is set to $\alpha = 6\times10^{-4}$Np/m and the fundamental frequency $\omega_a = 5\pi\times10^6$rad/s is fixed while $\omega_b = 4\pi\times10^6$rad/s (a) as well as $\omega_b = \pi\times10^6$rad/s (b). The initial conditions are chosen as $b_{ICa} = b_{ICb} = i7.5\times10^{-10}$m. All frequencies up to the 120th harmonic of each fundamental wave and all combination frequencies up to $60\omega_a \pm 60\omega_b$ are included.

where b_{dn} denotes the diffracted displacement amplitudes and is a function of x and y. Eventually, one can calculate the partial derivatives

$$\frac{\partial b_{dn}}{\partial x} = -\frac{ink_a}{2}\delta^2 b_n e^{ink_a\left(-\delta^2 x/2+\delta y\right)} + \frac{\partial b_n}{\partial x} e^{ink_a\left(-\delta^2 x/2+\delta y\right)} \tag{13}$$

and

$$\frac{i}{2nk_a}\frac{\partial^2 b_{dn}}{\partial y^2} = -\frac{ink_a}{2}\delta^2 b_n e^{ink_a\left(-\delta^2 x/2+\delta y\right)}. \tag{14}$$

Now, Eqs. (13) and (14) are combined and $\partial b_n/\partial x$ is substituted by the expression of Eq. (8) after applying the SVEA. This leads to

$$\frac{1}{2ink_a}\frac{\partial^2 b_{dn}}{\partial y^2} + \frac{\partial b_{dn}}{\partial x} = \frac{in\mu\omega_a}{Mc_r^3}\sum_{n=m+l} mlS_{ml} b_{dm} b_{dl} - \alpha n^2 b_{dn}. \tag{15}$$

The model obtained is very similar to the case of a single fundamental wave.[12] The main differences are again that n takes different values, and the formulation presented is written for the displacement amplitudes instead of the particle velocity amplitudes.

D. Simplified analytical model

1. General approach

In nonlinear ultrasonic experiments, having sufficiently large amplitudes of the frequency components under consideration is crucial to facilitate measurements with an improved SNR. In order to find combinations of initial fundamental amplitudes and frequencies that maximize the amplitudes of the second harmonics, and the sum and the difference frequency components, a general approach with a simplified model will be discussed as an alternative to a case-by-case investigation. The SVEA is applied and attenuation as well as diffraction effects are assumed to be negligible which is often a good approximation for small propagation distances. Additionally, for such distances the fundamentals are almost unaffected by other frequency components and they represent the only significant impact on the second harmonics, as well as on the sum and difference frequency components.

Based on these assumptions as well as based on Eqs. (8) and (15), the displacement amplitudes of the fundamentals become

$$\frac{\partial b_1}{\partial x} = 0 \rightarrow b_1 = b_{1Ca} = \text{constant}, \tag{16a}$$

$$\frac{\partial b_\phi}{\partial x} = 0 \rightarrow b_\phi = b_{1Cb} = \text{constant}. \tag{16b}$$

The displacement amplitudes of the second harmonics as well as of the sum and difference frequency components are given by

$$b_n = \frac{in\mu\omega_a x}{Mc_r^3}\sum_{n=m+l} mlS_{ml} b_m b_l, \tag{17}$$

where b_m and b_l solely represent fundamental displacement amplitudes. Thus, the second harmonics depend on the square of the corresponding fundamental displacement amplitude, whereas the sum and difference frequency components depend on the product of both fundamental displacement amplitudes. Consequently, the choice of the initial fundamental displacement amplitudes is evident—the product $|b_m b_l|$ should be maximized for the component of interest within the given experimental constraints, for example, by choosing an appropriate AMR.

Now, Eq. (17) is simulated in order to obtain recommendations on the choice of the fundamental frequencies for a specific setup with 7075-T651 aluminum[19] given in Table I. The results are depicted in Fig. 3. Here, it can be seen that the normalized slope of the $2\omega_b$ and the sum frequency components is larger for an increasing FMR, which is in line with Fig. 2. Moreover, as discussed in Sec. II B 2, a large difference frequency component is obtained when its own frequency and the fundamental frequencies are appropriately balanced. The illustrated curve of the difference frequency component within Fig. 3 is also in accordance with Fig. 2.

2. Sum and difference frequencies

In the following, two interesting effects are discussed. First, in Fig. 2(a), the sum frequency component has a steeper initial rise than the faster oscillating $2\omega_a$ component. The specific FMRs and AMRs for which the sum frequency component grows faster than the $2\omega_a$ component can be investigated with Eq. (17) which yields

$$\frac{b_{1+\phi}}{b_2} = \phi(1+\phi)\frac{(S_{1\phi}+S_{\phi 1})}{2S_{11}}\frac{b_\phi}{b_1}. \tag{18}$$

With $b_\phi = b_1$, the left curve in Fig. 4 is obtained for the aluminum given in Table I. Consequently, for a high enough FMR, it might be advantageous to consider the sum frequency component in an experiment.

Second, co-directional Rayleigh wave mixing can be attractive as it is possible to generate a difference frequency

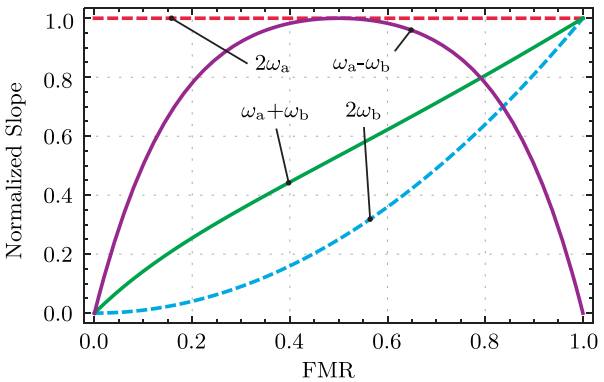

FIG. 3. (Color online) Slope $\partial b_n/\partial x$ normalized to the maxima and minima, respectively, of the corresponding frequency components. The frequency ω_a is kept constant while ω_b varies.

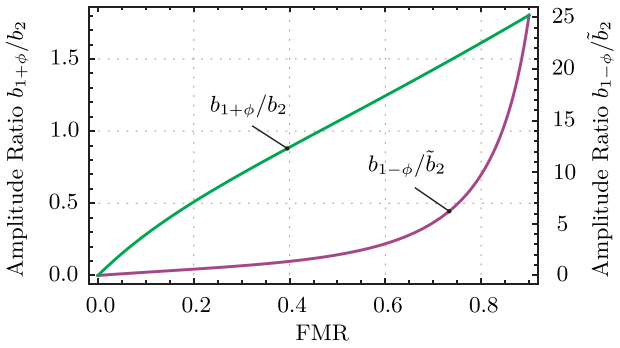

FIG. 4. (Color online) Amplitude ratios over the FMR.

component $b_{1-\phi}$ which grows much faster than a second harmonic $\tilde{b}_2$ of a single fundamental wave at the same frequency. By making use of Eq. (17) and by selecting the initial fundamental displacement amplitudes b_1 and $b_{-\phi}$ of the mixing case as half the initial fundamental displacement amplitude of the single wave case, the ratio

$$\frac{b_{1-\phi}}{\tilde{b}_2} = \frac{-\phi}{(1-\phi)} \frac{(S_{1,-\phi} + S_{-\phi 1})}{2S_{11}} \tag{19}$$

can be found. Note that a comma is introduced in $S_{1,-\phi}$ to clearly show that two different indices are involved. A simulation result is given in Fig. 4 for aluminum of Table I. It can be seen that for high FMRs the mixing method is clearly beneficial. The reason is that a high FMR in the mixing case implies much larger fundamental frequencies when compared to the case of a single fundamental wave. As a consequence, the energy transfer from the fundamentals is much higher in the former case, which finally leads to a larger ratio $b_{1-\phi}/\tilde{b}_2$.

E. Acoustic nonlinearity parameter

1. Modeling

One of the major objectives in nonlinear ultrasonic experiments is the measurement of the acoustic nonlinearity parameter (ANP) of a material. Therefore, the existing definition of the ANP within the literature[6,12] is extended to the case of co-directional Rayleigh wave mixing. By using the expression of the ANP for longitudinal waves analogously for Rayleigh waves, the definition

$$\beta = \frac{8b_2}{k_a^2 b_1^2 x} \tag{20}$$

in terms of the higher fundamental frequency is obtained which is based on and proportional to the definition by Herrmann *et al.*[6] As the ANP is a material property, a formulation can be specified which only depends on the solid under consideration. This is realized by inserting the displacement amplitudes b_1 and b_2 of a Rayleigh wave model into Eq. (20), at which the model is based on the same assumptions that led to this equation. These assumptions neglect both attenuation and diffraction effects, as well as assume a constant fundamental and a linearly changing second harmonic amplitude over the propagation distance.[13,20] Since all these points are incorporated within the simplified analytical model of Sec. II D, the corresponding displacement amplitudes are used to express the ANP only with material constants as

$$\beta_{mat} = \frac{16i\mu S_{11}}{Mc_r^2 k_a}, \tag{21}$$

which is given in a similar way by Shull *et al.*[12] Note that the wavenumber cancels out.

Now, for co-directional Rayleigh wave mixing, it might be desirable to calculate a similar ANP with both second harmonics as well as with the sum and difference frequency components. This results in a high flexibility in choosing the most attractive frequency component for a specific problem and the possibility to compare the results. In a fashion analogous to Eq. (20), the general expression for the four different ANPs is defined as

$$\beta_{ml} = \frac{16\,\mathrm{sgn}(ml) b_{m+l}}{(m+l) k_{|m|} k_{|l|} b_m b_l x}. \tag{22}$$

Here, m and l are either 1 or $\pm\phi$ and $m+l$ is 2, 2ϕ, $1+\phi$, or $1-\phi$. Moreover, $k_1 = k_a$ as well as $k_\phi = k_b$ and sgn denotes the sign function. Thus, β_{11} equals β of Eq. (20). Subsequently, β_{ml} is related to β. With Eq. (17), the general relationship between the different ANPs can be stated as

$$\beta = \beta_{ml} \frac{S_{11}}{\sum_{m+l=i+j} S_{ij}}. \tag{23}$$

The variable S_{ij} corresponds to S_{ml} with new control variables at which i and j are either 1 or $\pm\phi$.

2. Simulation

Next, the variation of the ANP β calculated in four different ways according to Eq. (23) is investigated when including the interaction, attenuation and diffraction effects. Therefore, Eq. (15) is simulated and Gaussian sources[16] of $s_a(y) = b_{1Ca} e^{-(y/r)^2}$ and $s_b(y) = b_{1Cb} e^{-(y/r)^2}$ are used for the corresponding fundamental waves. Here, a value of $r = 6.35$ mm is chosen which represents the radius of the wedge transducer utilized in Sec. IV for the experiments. At the limits in the y-direction, all the b_n's are set to zero.

The results of a simulation with the aluminum of Table I are presented in Fig. 5. Here, all curves are normalized to β_{mat}. Consequently, the four formulations of the ANP β yield indeed approximately the same absolute value of $|\beta_{mat}|$ at small propagation distances and deviate for larger propagation distances because of the interaction, attenuation, and diffraction effects. This confirms, on the one hand, the assumptions made in the simplified analytical model and, on the other hand, Eqs. (21) and (23) for small propagation distances which have been derived based on these assumptions. Thus, for such distances and measurements of absolute displacements, it might be possible to approximately obtain β_{mat} in four ways within an experiment.

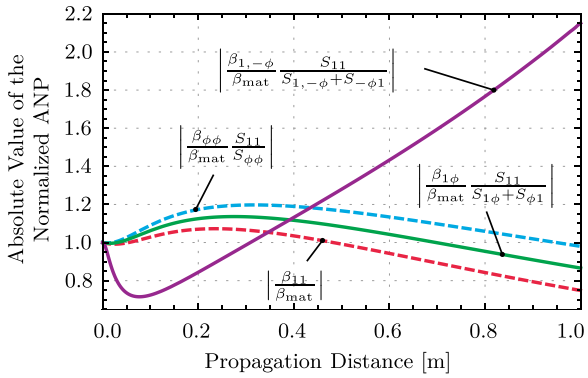

FIG. 5. (Color online) Absolute values of the normalized formulations of the ANP β at $y=0$ calculated with an attenuation coefficient of $\alpha=0.71$ Np/m and included diffraction effects. The fundamental frequencies are set to $\omega_a=4.666666\pi\times10^6$ rad/s and $\omega_b=3.733334\pi\times10^6$ rad/s, whereas $b_{\mathrm{IC}a}=b_{\mathrm{IC}b}=7.5\times10^{-10}$ m are chosen for the Gaussian sources. All frequencies up to the fourth harmonic of each fundamental wave and all combination frequencies up to $2\omega_a\pm2\omega_b$ are included.

In addition, in Fig. 5, the ANP formulations related to the second harmonics and the sum frequency component rise in the beginning as the diffraction effects are higher for lower frequencies. Consequently, the fundamentals are more reduced than the second harmonics and the sum frequency component. In contrast, as the difference frequency is much smaller than both of the fundamental frequencies, the corresponding ANP formulation initially drops. At larger distances attenuation becomes the dominant effect on the different curves.

III. FINITE ELEMENT MODEL

A. Modeling

As a next step, a simplified model using the finite element method (FEM) is set up with COMSOL MULTIPHYSICS 4.3a in order to validate a basic version of an analytical mixing model of Sec. II.

As the FEM is restricted by mesh resolution and time step sizes of the solver, it is not feasible to compare the analytical and finite element (FE) model in a case where high-frequency components have an essential influence on the results. Because of this and the fact that in an experiment, we are usually only interested in the fundamentals, the second harmonics as well as the sum and difference frequency components, the FE model is only used for propagation distances where other frequency components have insignificant amplitudes. Additionally, attenuation and diffraction effects are neglected. Consequently, a two dimensional FE model without attenuation is set up which resolves waves only up to the frequency $2\omega_a$. Accordingly, the FE model is compared to Eq. (8) for $\alpha=0$, in which only the fundamentals, second harmonics, as well as the sum and difference frequency components are included.

A sketch of the FE model is illustrated in Fig. 6. Here, the generation of Rayleigh waves with the wedge technique is applied which allows for mixing of the fundamentals already within the excitation signal. This signal consists of two sine waves with constant frequencies and amplitudes,

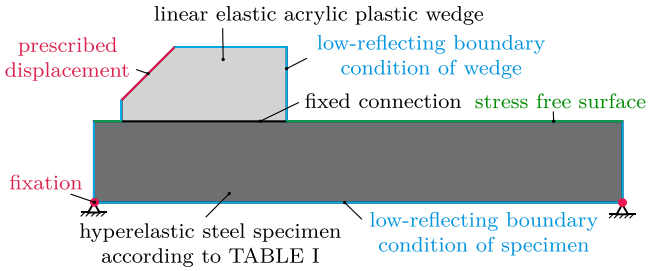

FIG. 6. (Color online) Sketch of the geometry, the material and the physics of the FE model.

which are added to obtain two co-directionally mixed longitudinal waves in the wedge and to eventually generate two co-directionally mixed Rayleigh waves in the specimen.

As the nonlinear effects we are interested in are small, it has proven of value to multiply the third order elastic constants (TOECs) by a relatively large positive factor in both the analytical and the FE model. Thus, one obtains significant amplitudes of the second harmonics as well as of the sum and difference frequency components at smaller propagation distances, which saves computational costs. The large amplitudes are important to obtain reasonable data within a discrete Fourier transform (DFT) of the measured time domain signal of the FE simulations. However, if the TOECs are increased too much, this will result in wave components other than the fundamentals, second harmonics, as well as the sum and difference frequency components, with amplitudes that are no longer negligible. A numerical analysis based on the analytical model led to a desired performance for a multiplication of the TOECs by a factor of 150 for the case of a propagation distance of around 20 mm, and the setups of the simulations of Sec. III B. Note that changing the TOECs is only possible because the objective of this study is to compare the behavior of both models, and not necessarily to use realistic material parameters. Also, the strains stay small. Moreover, the hyperelastic material model based on Murnaghan is used which is predefined in the nonlinear structural materials module of COMSOL.

Quadratic elements are selected, and the mesh size is chosen around five times smaller than the smallest wavelength under consideration, which is based on ω_a for the wedge and $2\omega_a$ for the specimen.

B. Simulation

For the simulation, a time dependent study is chosen using the Pardiso solver as well as a Courant–Friedrichs–Lewy number of around 0.2.

In order to compare the analytical and the FE model, the time domain signal of the vertical displacements is extracted within COMSOL at 32 points on the stress free surface of the specimen. Note that the horizontal displacements lead to the same qualitative results. As a next step, a Hann window is applied to a steady-state portion of the measured time domain signal and a DFT is utilized. Eventually, the amplitudes at the six frequencies considered in the frequency domain are used to calculate the corresponding amplitudes in the time domain, with the empirical formula

$$\text{time domain amplitude} = \frac{4 \times \text{frequency domain amplitude}}{\text{number of data points used for Hann window}} \tag{24}$$

similar to the literature.[21] This equation holds for the common DFT convention for signal processing which can be found, for example, in the MATHEMATICA 9 documentation. Subsequently, the amplitudes of the fundamentals of the analytical model are fitted to the data of the FEM simulation by adjusting the initial fundamental displacement amplitudes. Nevertheless, the second harmonics as well as the sum and difference frequency components are solely calculated by solving the differential equations of the analytical model.

The results of two comparisons between both models are shown in Fig. 7. Here, the scale on the left-hand side holds for the fundamentals, while the scale on the right-hand side holds for the other components. The amplitudes of the sine waves for the excitation within the wedge are selected in order to obtain fundamental Rayleigh wave displacements which are of the same dimension as experimental data for longitudinal waves.[17] Moreover, roughly the point where the center of the excited longitudinal wave beam hits the specimen is chosen as the origin of the Rayleigh wave to obtain a meaningful fit.

From Fig. 7, one can infer that both models match relatively well for various FMRs and AMRs within the propagation distances examined. However, differences can be seen

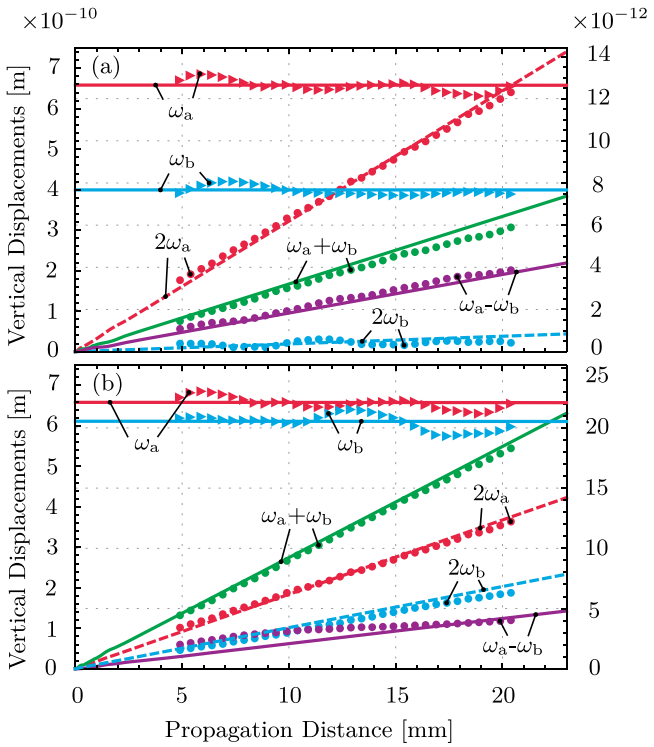

FIG. 7. (Color online) Vertical displacements related to different frequencies of the analytical (curves) and the FE model (markers) at the stress free surface. The fundamental frequencies are chosen as $\omega_a = 5\pi \times 10^6$ rad/s and $\omega_b = 2\pi \times 10^6$ rad/s (a) as well as $\omega_b = 4\pi \times 10^6$ rad/s (b). The excitation of the mixed longitudinal wave in the wedge is conducted with two sine signals at amplitudes of 15×10^{-10} m.

which are caused among others by the following discrepancies.

(1) Rayleigh wave generation with the wedge technique in the FE model, versus source displacement amplitudes for Rayleigh waves in the analytical model.
(2) Signal transformation with a DFT for the FE model versus no transformation for the analytical model.
(3) Finite domains with low reflections in the FE model versus a semi-infinite solid without reflections in the analytical model.

In addition, a comparison between plots (a) and (b) clearly shows that the amplitude of the ω_b component tends to increase for higher frequencies, although the excitation amplitudes within the wedge do not change. This effect is possibly related to the fact that the energy of a Rayleigh wave with a higher frequency is shifted more closely to the surface.[9]

Finally, there is still some potential to obtain more accurate data from the FEM. For example, larger domains could weaken the effects from reflections in order to reduce the oscillations of the fundamentals within Fig. 7. Nevertheless, the objective of a basic comparison between the two models is accomplished, and the analytical results are qualitatively validated with the FEM for the propagation distances under consideration.

IV. EXPERIMENTS

A. Experimental setup and procedure

Now, the mixing technique for two co-directional Rayleigh waves is implemented experimentally. The setup and utilized instruments of the conducted experiments are almost identical to that of Thiele *et al.*[22] with the difference that two signal sources (80 MHz 33250A function generators from Agilent) instead of one are used. In this research, the signal sources generate two sine waves with individual frequencies and amplitudes which are added in the signal to a contact transducer on a wedge with a nominal center frequency of 2.25 MHz. This launches two co-directionally mixed Rayleigh waves in the specimen under consideration, analogous to the situation described in Sec. III. The specimen is made of the aluminum given in Table I. The receiver is a non-contact, air-coupled transducer (Ultran NCT4-D13) with a nominal center frequency of 4 MHz. Details about the experimental setup and the utilized instruments such as the transducers are given by Thiele *et al.*[22]

The experiments performed investigate the fundamentals, second harmonics as well as the sum and difference frequency components. To obtain information about the development of these frequency components, measurements are conducted at different propagation distances.

B. Experimental results

1. Experimental feasibility

With the single narrow band exciting transducer utilized, it is usually recommended to select a high FMR and fundamental frequencies close to the transducer center frequency.

Nevertheless, the FMR should not be too close to a value of one in order to avoid overlaps between the frequency components considered in the DFT. Thus, the fundamental frequencies of Sec. II E 2 which are $f_a = 2.333333$ MHz and $f_b = 1.866667$ MHz are used for all following experiments [with $f = \omega/(2\pi)$]. In addition, as it was not possible to measure meaningful data for the difference frequency component with the present setup due to bandwidth limitations of the receiving transducer, the experiments focus solely on the fundamentals, second harmonics and the sum frequency component.

The procedure for the data processing is similar to Thiele *et al.*[22] Initially, a time domain signal is measured at the center of the wave beam. Based on this, a Hann window and the DFT lead to a frequency domain representation such as in Fig. 8, where the amplitudes have been back calculated to the time domain with Eq. (24). Note that the utilized air-coupled transducer measures the amplitude of the leaked longitudinal wave in the air in volts which is approximately proportional to the particle displacements in the material and will therefore be used in the same sense throughout this section. In addition, the maxima of the frequency components considered in Fig. 8 cannot be directly compared to each other because of the frequency response of the receiving transducer.

As a next step, these maxima are determined at propagation distances from 30 to 78 mm in 1 mm increments, which yields Fig. 9. Here, some typical characteristics can be observed—the fundamentals transfer their energy to the other frequency components and get attenuated as well as diffracted leading to a decrease in amplitude. In contrast, the second harmonics and the sum frequency component rise essentially. However, as the measurements are conducted in the far field, attenuation as well as diffraction effects tend to significantly decrease the wave generation of these components at larger propagation distances.

Subsequently, in Fig. 10 the ANP formulas of Eq. (22) multiplied by x are used. At this, the measured amplitudes in volts are representatively used for the displacement amplitudes, which only gives relative ANPs. In addition, the scale

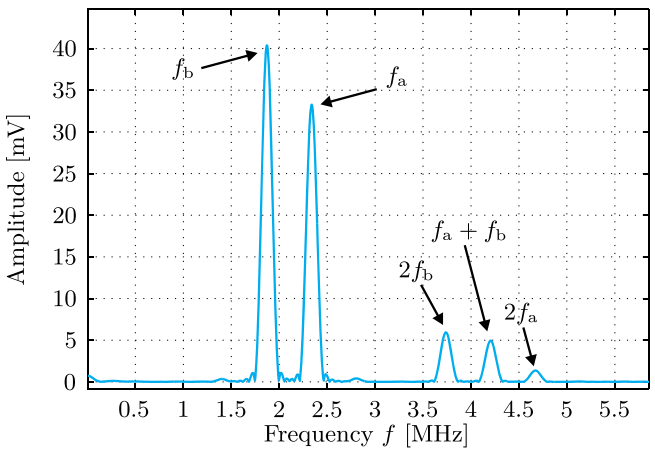

FIG. 8. (Color online) DFT of the time domain signal measured at 78 mm propagation distance with a Hann window applied to a steady state portion. Both function generator outputs are set to 700 mVpp. [Note, for example, that $f_a = \omega_a/(2\pi)$, etc.]

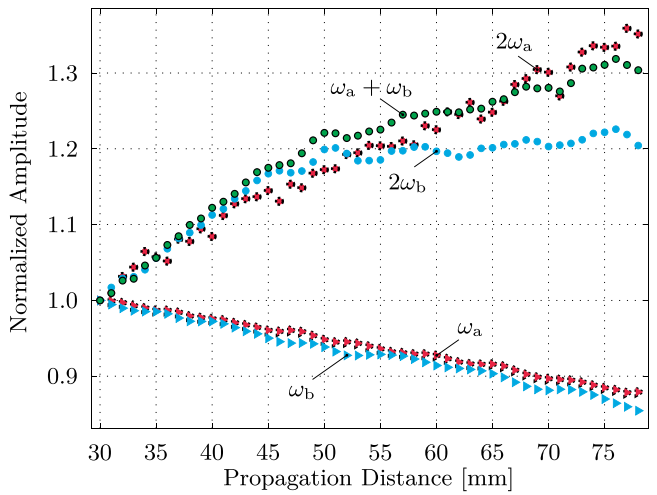

FIG. 9. (Color online) Amplitudes of different frequency components over the propagation distance normalized to their value at 30 mm. Both function generator outputs are set to 700 mVpp.

on the right-hand side solely holds for β_{11} and for the qualitative investigations of this research, only one set of measurements is conducted because of the high repeatability.[22]

Thiele *et al.*[22] used the same propagation distances and a similar fundamental frequency to examine second harmonic generation with a single fundamental, where they observed a relatively constant behavior for the ANP. Also, it can be inferred from the simulations of Fig. 5, where the attenuation coefficient of the ω_a component and the frequencies of the experiment have been used, that the behavior of the three considered ANPs should also be approximately constant for the propagation distances under consideration. Note that as the initial fundamental amplitudes in the analytical investigations could be relatively different from the experiments, the simulations are supposed to be only utilized as an orientation. Nevertheless, useful measurements should allow for acceptable linear fits with the different ANPs as

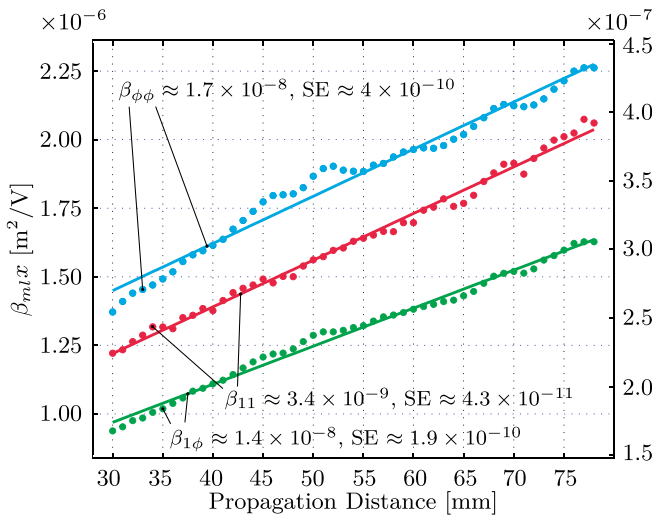

FIG. 10. (Color online) Different ANPs times propagation distance x for experimental data (markers). The slopes of the corresponding linear fits (lines) and the standard errors (SE) in m^2/(Vmm) are specified. Both function generator outputs are set to 700 mVpp.

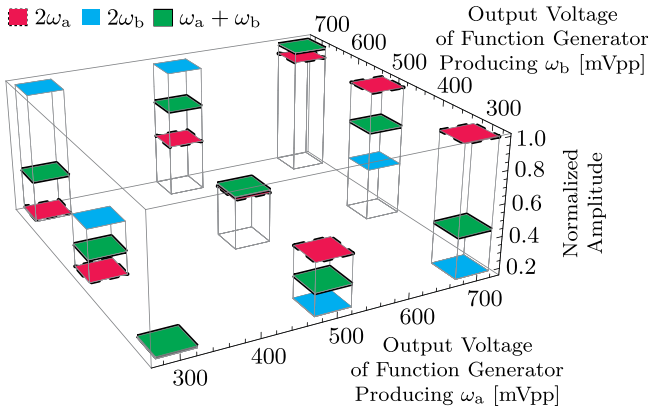

FIG. 11. (Color online) Average amplitudes normalized to the maximum of the corresponding frequency component for different output voltages of the function generators.

corresponding slopes. In fact, the linear fits within Fig. 10 are reasonable.

Thus, it can be concluded that co-directional Rayleigh wave mixing is experimentally feasible in order to obtain a meaningful relative measure of the acoustic nonlinearity of a material in at least three different ways.

2. Variation of initial fundamental amplitudes

Finally, a set of ultrasonic measurements is performed to determine if the theory is in accordance with the behavior of the experimental setup for variations of the output voltage of the function generators. A range from 300 to 700 mVpp is selected for which the overall setup behaves relatively linearly. Thus, the initial fundamental amplitudes are approximately proportional to the output voltage of the corresponding function generator. One set of measurements is conducted for each combination of output voltages for propagation distances from 30 to 78 mm at increments of 4 mm.

In Fig. 11 the results of the average amplitudes over the propagation distance of the second harmonics and the sum frequency component are shown. The second harmonics scale approximately with the square of the corresponding initial fundamental amplitude, and function generator output voltage, respectively. The sum frequency component increases nearly linearly, but in both axis directions.

The experimental dependence of the second harmonics and the sum frequency component on the initial fundamental amplitudes is similarly predicted by theoretical investigations—for example, by the quasilinear theory for a Gaussian source of Shull *et al.*[12] when applied to the problem under consideration, or by Eq. (17) for small propagation distances.

V. CONCLUSION

This paper demonstrates a variety of effects and possibilities concerning the mixing of two co-directional Rayleigh waves in a weakly nonlinear solid by using analytical models, FEM simulations and experiments.

First, the existing nonlinear theory for a single fundamental Rayleigh wave[9,12] is extended to the case of co-directional mixing of two Rayleigh waves. Simulation models are developed which incorporate interaction as well as attenuation and diffraction effects. Shock plus pulse formations in the waveforms of the particle velocities and the development of the displacement amplitudes of the fundamentals, second harmonics, as well as of the sum and difference frequency components as a function of the propagation distance are investigated. General recommendations on the choice of the mixing parameters (FMR and AMR) in order to maximize the second harmonics as well as the sum and difference frequency components are given. Also, an important advantage of the difference frequency component when compared to the second harmonic of a single fundamental wave is discussed. Furthermore, ANPs for the second harmonics as well as for the sum and difference frequency components are formulated, and related to each other in order to specify the same ANP in four different ways.

Moreover, a basic version of the analytical model is validated with a FEM simulation. In the end, experiments show that meaningful data for the ANPs related to the second harmonics and the sum frequency component can be measured for co-directional Rayleigh wave mixing. This allows the monitoring of the material state in different ways which can be beneficial.

A next step is to confirm the proposed experimental mixing technique with a study using different materials and specimens.

ACKNOWLEDGMENTS

This research was performed using funding received from the DOE Office of Nuclear Energy's Nuclear Energy University Programs and NST through CMMI-1363221 and CMMI-1362204. The German Academic Exchange Service (DAAD) and the Friedrich-Ebert-Foundation (FES) supported this work through fellowships to M.B.M. The authors want to thank Sebastian Thiele who installed the experimental setup.

[1]J. H. Cantrell, "Substructural organization, dislocation plasticity and harmonic generation in cyclically stressed wavy slip metals," Proc. R. Soc. London, Ser. A **460**, 757–780 (2004).
[2]J.-Y. Kim, L. J. Jacobs, J. Qu, and J. W. Littles, "Experimental characterization of fatigue damage in a nickel-base superalloy using nonlinear ultrasonic waves," J. Acoust. Soc. Am. **120**, 1266–1273 (2006).
[3]M. Liu, G. Tang, L. J. Jacobs, and J. Qu, "Measuring acoustic nonlinearity parameter using collinear wave mixing," J. Appl. Phys. **112**, 024908 (2012).
[4]A. J. Croxford, P. D. Wilcox, B. W. Drinkwater, and P. B. Nagy, "The use of non-collinear mixing for nonlinear ultrasonic detection of plasticity and fatigue," J. Acoust. Soc. Am. **126**, EL117–EL122 (2009).
[5]G. L. Jones and D. R. Kobett, "Interaction of elastic waves in an isotropic solid," J. Acoust. Soc. Am. **35**, 5–10 (1963).
[6]J. Herrmann, J.-Y. Kim, L. J. Jacobs, J. Qu, J. W. Littles, and M. F. Savage, "Assessment of material damage in a nickel-base superalloy using nonlinear Rayleigh surface waves," J. Appl. Phys. **99**, 124913 (2006).
[7]S. V. Walker, J.-Y. Kim, J. Qu, and L. J. Jacobs, "Fatigue damage evaluation in A36 steel using nonlinear Rayleigh surface waves," NDT&E Int. **48**, 10–15 (2012).
[8]N. Kalayanasundaram, "Nonlinear mode coupling of surface acoustic waves on an isotropic solid," Int. J. Eng. Sci. **19**, 435–441 (1981).
[9]E. A. Zabolotskaya, "Nonlinear propagation of plane and circular Rayleigh waves in isotropic solids," J. Acoust. Soc. Am. **91**, 2569–2575 (1992).
[10]E. A. Zabolotskaya, "Nonlinear propagation of Rayleigh waves," Opt. Acoust. Rev. **1**, 133–140 (1990).
[11]N. Kalyanasundaram, "Coupled amplitude theory of nonlinear surface acoustic waves," J. Acoust. Soc. Am. **72**, 488–493 (1982).

[12]D. J. Shull, E. E. Kim, M. F. Hamilton, and E. A. Zabolotskaya, "Diffraction effects in nonlinear Rayleigh wave beams," J. Acoust. Soc. Am. **97**, 2126–2137 (1995).
[13]J. H. Cantrell and T. Kundu, *Ultrasonic Nondestructive Evaluation: Engineering and Biological Material Characterization - Fundamentals and Applications of Nonlinear Ultrasonic Nondestructive Evaluation* (CRC Press, Boca Raton, FL, 2003), pp. 363–433.
[14]R. Bonifacio, R. Caloi, and C. Maroli, "The slowly varying envelope approximation revisited," Opt. Commun. **101**, 185–187 (1993).
[15]R. N. Thurston, "Interpretation of ultrasonic experiments on finite-amplitude waves," J. Acoust. Soc. Am. **41**, 1112–1125 (1967).
[16]D. J. Shull, M. F. Hamilton, Y. A. Il'insky, and E. A. Zabolotskaya, "Harmonic generation in plane and cylindrical nonlinear Rayleigh waves," J. Acoust. Soc. Am. **94**, 418–427 (1993).
[17]D. J. Barnard, "Variation of nonlinearity parameter at low fundamental amplitudes," Appl. Phys. Lett. **74**, 2447–2449 (1999).
[18]Y. V. Kopylov, A. V. Popov, and A. V. Vinogradov, "Application of the parabolic wave equation to x-ray diffraction optics," Opt. Commun. **118**, 619–636 (1995).
[19]D. M. Stobbe, "Acoustoelasticity in 7075-T651 aluminum and dependence of third order elastic constants on fatigue damage," Master's thesis, Georgia Institute of Technology, Atlanta, GA, 2005.
[20]J.-Y. Kim, L. J. Jacobs, J. Qu, and T. Kundu, *Ultrasonic and Electromagnetic NDE for Structure and Material Characterization: Engineering and Biomedical Applications—Material Characterization by Nonlinear Ultrasonic Technique* (CRC Press, Boca Raton, FL, 2012), pp. 395–456.
[21]A. Girgis and F. Ham, "A quantitative study of pitfalls in the FFT," IEEE Trans. Aero. Electr. Syst. **AES-16**, 434–439 (1980).
[22]S. Thiele, J.-Y. Kim, J. Qu, and L. J. Jacobs, "Air-coupled detection of nonlinear Rayleigh surface waves to assess material nonlinearity," Ultrasonics **54**, 1470–1475 (2014).